nature genetics

Inactivating mutations in *MFSD2A*, required for omega-3 fatty acid transport in brain, cause a lethal microcephaly syndrome

Alicia Guemez-Gamboa[1,2,11], Long N Nguyen[3,11], Hongbo Yang[4,11], Maha S Zaki[5], Majdi Kara[6], Tawfeg Ben-Omran[7], Naiara Akizu[1,2], Rasim Ozgur Rosti[1,2], Basak Rosti[1,2], Eric Scott[1,2], Jana Schroth[1,2], Brett Copeland[1,2], Keith K Vaux[1,2], Amaury Cazenave-Gassiot[8], Debra Q Y Quek[3], Bernice H Wong[3], Bryan C Tan[3], Markus R Wenk[8], Murat Gunel[9], Stacey Gabriel[10], Neil C Chi[4], David L Silver[3] & Joseph G Gleeson[1,2]

Docosahexanoic acid (DHA) is the most abundant omega-3 fatty acid in brain, and, although it is considered essential, deficiency has not been linked to disease[1,2]. Despite the large mass of DHA in phospholipids, the brain does not synthesize it. DHA is imported across the blood-brain barrier (BBB) through the major facilitator superfamily domain–containing 2a (MFSD2A) protein[3]. MFSD2A transports DHA as well as other fatty acids in the form of lysophosphatidylcholine (LPC). We identify two families displaying *MFSD2A* mutations in conserved residues. Affected individuals exhibited a lethal microcephaly syndrome linked to inadequate uptake of LPC lipids. The *MFSD2A* mutations impaired transport activity in a cell-based assay. Moreover, when expressed in *mfsd2aa*-morphant zebrafish, mutants failed to rescue microcephaly, BBB breakdown and lethality. Our results establish a link between transport of DHA and LPCs by MFSD2A and human brain growth and function, presenting the first evidence of monogenic disease related to transport of DHA in humans.

The two affected families, one from Libya and the other from Egypt, presented with microcephaly, developmental delay and intellectual disability, among other clinical characteristics, including hypotonia, hyperreflexia, spastic quadriparesis, seizures and ultimately death within the first few years of life (**Supplementary Table 1**). Consistent with a recessive mode of inheritance, both families demonstrated first-cousin parental consanguinity, each with two affected members (**Fig. 1a**), and there were not other non-genetic risk factors that would account for symptoms[4]. Brain imaging studies showed gross hydrocephalus, with hugely dilated lateral ventricles, effacement of the cortical surface, and cerebellar and brainstem hypoplasia and/or atrophy (**Fig. 1b**). We performed exome sequencing on both families and identified two rare protein-altering homozygous variants in the *MFSD2A* gene (NM_032793.4) (**Supplementary Figs. 1** and **2**). Family 1825 presented a g.40431005C>T variant on chromosome 1, leading to a c.476C>T nucleotide change and corresponding p.Thr159Met protein change. Family 1422 harbored a g.40431162C>T variant on chromosome 1, leading to a c.497C>T nucleotide change and corresponding p.Ser166Leu protein change (**Fig. 1c**,**d**). Both variants were predicted to be highly damaging using standard programs (**Supplementary Tables 2** and **3**), and the altered amino acid residues have been conserved throughout vertebrate evolution (**Fig. 1e**). Both mutations were in constitutively spliced exons and segregated in the respective families according to a fully penetrant, recessive mode of inheritance (**Supplementary Fig. 3**). Moreover, exome sequencing results from both affected individuals showed no rare deleterious homozygous variants in any gene listed in the Online Mendelian Inheritance in Man (OMIM) database to cause clinically relevant disease (**Supplementary Tables 4** and **5**).

MFSD2A encodes a 12-pass transmembrane protein whose homolog in mouse was recently shown to be required for brain uptake of LPCs containing DHA and other fatty acids and has been implicated in the formation of the BBB[3,5]. MFSD2A is highly enriched in cerebral vasculature where it is exclusively found in the endothelium constituting the BBB[3,5,6], a localization pattern we documented, and it colocalized with GLUT1, a marker for endothelial cells in the BBB, in control human brain samples (**Supplementary Fig. 4**). Moreover, *MFSD2A* transcripts were expressed in a range of human tissues (**Supplementary Fig. 5**), but function in other organs has not been described. We introduced the mutations encoding p.Thr159Met and p.Ser166Leu into human *MFSD2A* cDNA, expressed these constructs

[1]Department of Neurosciences, University of California, San Diego, La Jolla, California, USA. [2]Howard Hughes Medical Institute, Chevy Chase, Maryland, USA. [3]Signature Research Program in Cardiovascular and Metabolic Disorders, Duke–National University of Singapore Graduate Medical School, Singapore. [4]Department of Medicine, University of California, San Diego, La Jolla, California, USA. [5]Clinical Genetics Department, Human Genetics and Genome Research Division, National Research Centre, Cairo, Egypt. [6]Department of Pediatrics, Tripoli Children's Hospital, Tripoli, Libya. [7]Clinical and Metabolic Genetics Division, Department of Pediatrics, Hamad Medical Corporation, Doha, Qatar. [8]Department of Biochemistry, National University of Singapore, Singapore. [9]Yale Program on Neurogenetics, Departments of Neurosurgery, Neurobiology and Genetics, Yale University, School of Medicine, New Haven, Connecticut, USA. [10]Broad Institute of MIT and Harvard, Cambridge, Massachusetts, USA. [11]These authors contributed equally to this work. Correspondence should be addressed to J.G.G. (jogleeson@rockefeller.edu) or D.L.S. (david.silver@duke-nus.edu.sg).

Received 10 September 2014; accepted 30 April 2015; published online 25 May 2015; doi:10.1038/ng.3311

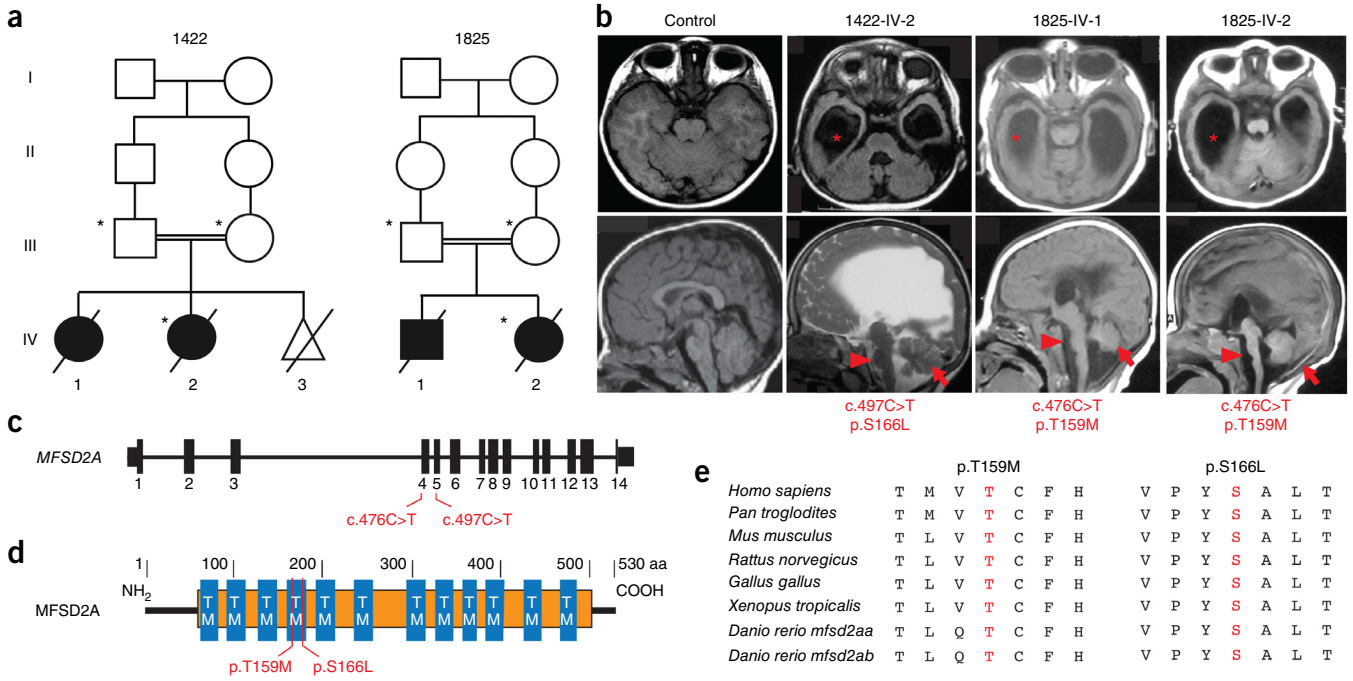

Figure 1 *MFSD2A* mutations cause severe microcephaly and ventriculomegaly. (**a**) Consanguineous families 1422 and 1825. Circle, female; square, male; diagonal line, deceased; triangle, spontaneous abortion; asterisk, individual sampled. (**b**) Top, axial MRI. Bottom, parasagittal MRI. Images show enlarged lateral ventricles (asterisks) and hypoplasia of the corpus callosum, brain stem (arrowheads) and cerebellum (arrows) in affected children. (**c**) Exonic structure of *MFSD2A* with the location of the mutations identified in patients. (**d**) Location of altered residues relative to the predicted protein. The major facilitator superfamily general substrate transporter domain is shown in orange; TM, transmembrane domain. (**e**) Alignment of the amino acid sequences of vertebrate MFSD2A proteins, showing the conservation of residues Thr159 and Ser166.

in HEK293 cells, and examined protein expression and localization by immunoblot and immunofluorescence analyses. Both mutant proteins were expressed at similar levels and showed reported post-translational modifications[7] that were identical to those for wild-type protein (**Fig. 2a**). Furthermore, both mutant proteins were stably expressed and localized to the plasma membrane in a fashion similar to wild-type protein (**Fig. 2b**), suggesting that the p.Thr159Met and p.Ser166Leu alterations do not destabilize the protein. To test for functional impairment, we used a cell-based assay with a range of concentrations of exogenous LPC-[^{14}C]DHA, LPC-[^{14}C]oleate and LPC-[^{3}H]palmitate substrates after transfection of the *MFSD2A* constructs into

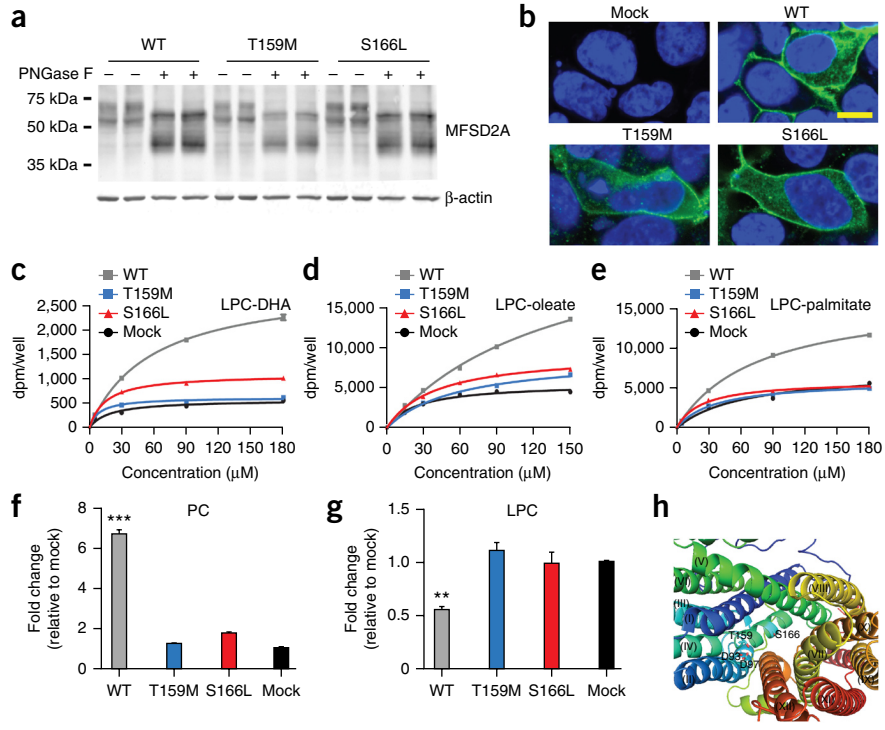

Figure 2 Thr159Met and Ser166Leu MFSD2A mutants display impaired LPC transport. (**a**,**b**) Immunoblotting (**a**) and immunolocalization (**b**) of wild-type (WT) MFSD2A and the Thr159Met and Ser166Leu mutants expressed in HEK293 cells. PNGase F is an endoglycosidase that specifically removes N-linked glycans from glycoproteins. Green, MFSD2A; blue, DAPI. Scale bar, 10 μm. (**c**–**e**) Concentration-dependent transport of LPC-[^{14}C]DHA (**c**), LPC-[^{14}C]oleate (**d**) and LPC-[^{3}H]palmitate (**e**) after 30 min (measured in disintegrations per minute (dpm)/well) in HEK293 cells expressing wild-type MFSD2A or the Thr159Met or Ser166Leu mutant. Results are shown from representative experiments. (**f**,**g**) Quantification of the radiolabeled PC (**f**) and LPC (**g**) bands from the thin-layer chromatography (TLC) plates shown in **Supplementary Figure 6**. (**h**) View of the internal cavity of human MFSD2A. Roman numerals are α-helix numbers. Experiments in **c**–**g** were performed twice in triplicate. Data in **f** and **g** are expressed as means ± s.e.m. $^{***}P < 0.001$, $^{**}P < 0.01$. Specific P values from left to right: $P < 0.001$, $P = 0.0026$, $P = 0.0019$.

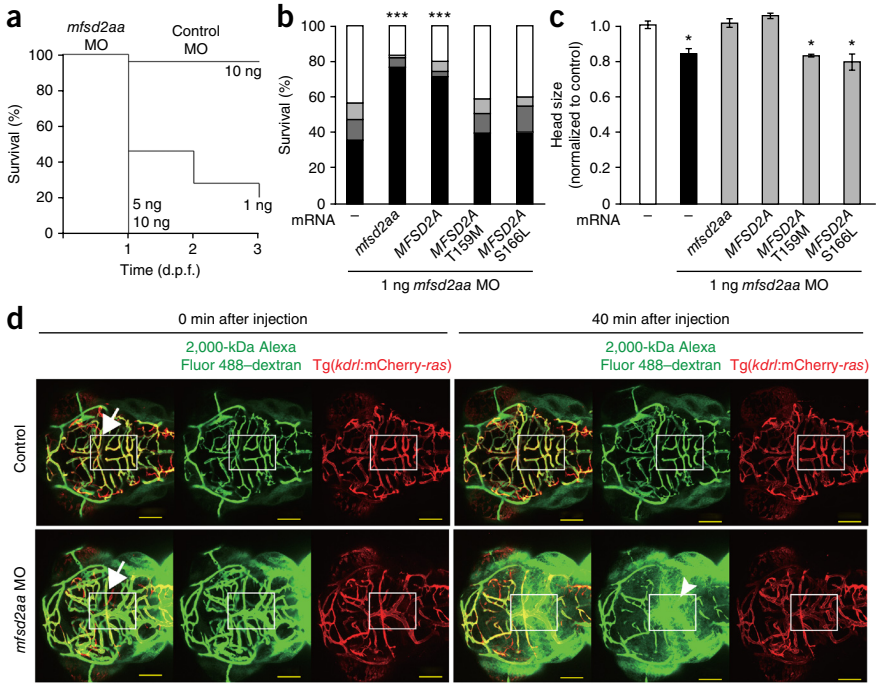

Figure 3 Zebrafish *mfsd2aa* morphants show disrupted BBB integrity, lethality and microcephaly. (**a**) Kaplan-Meier plot of the survival of *mfsd2aa* morphants ($n = 457$ embryos) and control morphants (scrambled morpholino oligonucleotide (MO); $n = 105$ embryos). (**b**) *mfsd2aa* morpholino (1 ng) was coinjected with wild-type zebrafish *mfsd2aa* mRNA (50 ng; $n = 118$ embryos), wild-type human *MFSD2A* mRNA (50 ng; $n = 135$ embryos), or human *MFSD2A* mRNA encoding the Thr159Met or Ser166Leu mutant (50 ng; $n = 120$ and 107 embryos, respectively). Bars represent the cumulative percentages of survival at 1 (dark gray), 2 (light gray) and 3 (black) d.p.f. (**c**) Comparison of the head sizes of control and *mfsd2aa* morphants ($n = 20$ embryos each). Data are expressed as means ± s.e.m. (**d**) Intracardiac injection of 2,000-kDa dextran into *mfsd2aa* morpholino–injected and control embryos. Arrows, colocalization of dextran (green) and cranial blood vessels (red). The arrowhead indicates dextran extravasation into the brain parenchyma. Scale bars, 100 µm. $^{***}P < 0.001$, $^{*}P < 0.05$. Specific P values in **b** and **c** from left to right: $P < 0.001$, $P < 0.001$, $P = 0.0143$, $P = 0.0302$, $P = 0.0310$.

HEK293 cells (**Fig. 2c–e**). Both mutants exhibited transport activity similar to the background level in mock-transfected cells for all LPC lipids tested, indicating impaired LPC transporter activity. LPCs taken up by cells are esterified into phosphatidylcholine (PC) by cellular lysophosphatidylcholine acyltransferase (LPCAT) enzymes[8]. Thus, we assessed cells transfected with the *MFSD2A* constructs for conversion of labeled LPCs to PC (**Fig. 2f,g** and **Supplementary Fig. 6**). Cells expressing wild-type MFSD2A showed significantly greater ($P < 0.01$) conversion of exogenous LPCs into membrane PC than cells expressing the Thr159Met and Ser166Leu MFSD2A mutants, consistent with loss of transport function in mutants.

We inferred a molecular explanation for loss of function with the mutations from the recently solved atomic-resolution structure of MelB[9,10], the *Escherichia coli* sodium-melibiose transporter that is ~54% similar to MFSD2A, making it a suitable candidate for modeling the substitutions identified in patients. Thr159 is homologous to Thr121 in MelB, which was shown to hydrogen bond with aspartate residues Asp93 and Asp97, essential for sodium binding and critical for transport activity (**Fig. 2h** and **Supplementary Note**). In contrast, Ser166 was not conserved in *E. coli* but was located at the putative substrate-binding site as predicted by the MelB structure. Therefore, both mutations are predicted to interfere with transport activity (**Fig. 2h** and **Supplementary Note**).

To validate the functional impact of the human mutations *in vivo*, we developed a zebrafish model of *MFSD2A* deficiency. *MFSD2A* has two paralogs in zebrafish, *mfsd2aa* and *mfsd2ab*, encoding proteins with 58% and 62% identity to the human amino acid sequence, respectively. Whole-mount *in situ* hybridization showed expression of *mfsd2aa* and *mfsd2ab* mRNA transcripts throughout the developing nervous system (**Supplementary Fig. 7**). As expected from their high level of amino acid sequence identity with the human protein, Mfsd2aa and Mfsd2ab exhibited similar transport activity for LPC ligands, at levels similar to those seen with human MFSD2A (**Supplementary Fig. 8**). We thus tested the genetic consequences of the human mutations by knocking down endogenous *mfsd2aa* and *mfsd2ab* using morpholino oligonucleotides. We observed lethality with each *mfsd2aa* and *mfsd2ab* morpholino, indicating that the encoded transporters have non-redundant roles and are required for survival (**Fig. 3a** and **Supplementary Fig. 9**). Lethality in morphants is also consistent with postnatal lethality in humans and mice with MFSD2A deficiency (40% of *Mfsd2a*-knockout mice die postnatally[7]). However, as the majority of *mfsd2aa* and *mfsd2ab* morphants died before neural maturation (the BBB forms at 3 days post-fertilization (d.p.f.) in zebrafish[11]), it is unlikely that lethality is caused solely by disruption of neural function.

Remarkably, even at a dose of 1 ng of *mfsd2aa* morpholino, about 50% of morphants died by 1 d.p.f., with only ~20% remaining by 3 d.p.f. (**Fig. 3a** and **Supplementary Fig. 9**). Because the observed lethal phenotype in fish at 1 d.p.f. was more severe than the phenotypes in humans and mice, other species-specific effects of Mfsd2aa and Mfsd2ab depletion that are unrelated to lipid transport cannot be excluded. Given that *mfsd2aa* and *mfsd2ab* morphants both showed lethality, we focused our genetic tests arbitrarily on *mfsd2aa*. To corroborate the pathogenicity of the human mutations, we coinjected mRNA for wild-type or mutated human *MFSD2A* or wild-type zebrafish *mfsd2aa* into zebrafish zygotes together with *mfsd2aa* morpholino. We observed that either zebrafish or human wild-type mRNA largely rescued the lethal phenotype, whereas coinjection with human *MFSD2A* mRNA encoding the Thr159Met or Ser166Leu mutant failed to reverse the lethality (**Fig. 3b**). Moreover, *mfsd2aa* morphants presented with microcephaly similar to human subjects with *MFSD2A* mutations, and, whereas wild-type zebrafish or human mRNA rescued this phenotype, human *MFSD2A* mRNA encoding the Thr159Met or Ser166Leu mutant did not (**Fig. 3c**), providing further support for the genetic causality of the human mutations. However, morphant phenotypes may include off-target effects[12], so additional studies of germline mutants will be needed to validate the observed phenotypes.

MFSD2A has been implicated in the formation of the BBB, as demonstrated by increased uptake of fluorescently labeled dextran

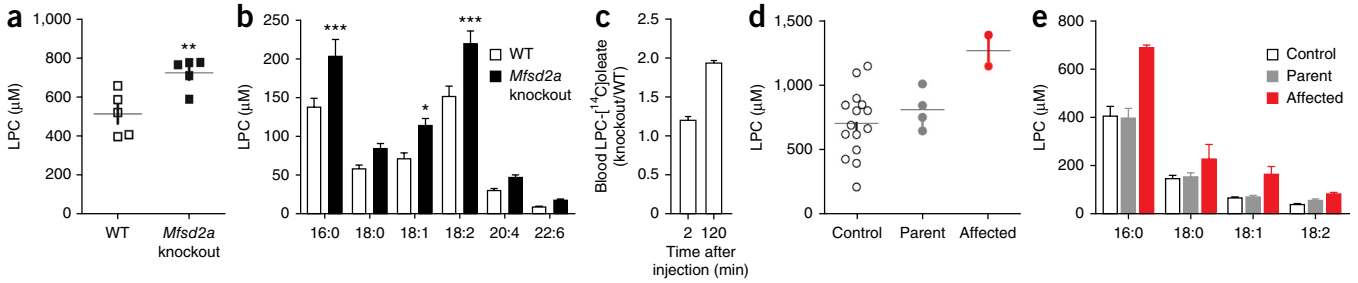

Figure 4 Total plasma LPC levels and levels of individual LPC species by lipidomic mass spectrometry. (**a**,**b**) Concentrations of total LPC (**a**) and common LPC species with a chain length of 16–22 carbons (**b**) in plasma from wild-type ($n = 5$) and *Mfsd2a*-knockout ($n = 5$) mice, with 3 technical replicates. (**c**) Quantification of injected LPC-[^{14}C]oleate over time in the plasma of *Mfsd2a*-knockout mice ($n = 4$) relative to wild-type littermates ($n = 3$). (**d**,**e**) Total plasma LPC concentrations (**d**) and concentrations of common LPC species (**e**) for the affected individuals from families 1422 and 1825 and their unaffected parents, as well as age-matched controls. Analysis was performed once with three technical replicates from two independent plasma samples collected on different days. Error bars, s.d. In **a** and **d**, horizontal bars represent median values. $^{***}P < 0.001$, $^{**}P < 0.01$, $^{*}P < 0.05$. Specific P values in **a** and **b** from left to right: $P = 0.0094$, $P = 0.0004$, $P = 0.0372$, $P = 0.0002$.

beads through vesicular transport into the brain parenchyma of *Mfsd2a*-knockout mice[5]. Given this finding, we tested whether *mfsd2aa*-morphant zebrafish showed disruption of the BBB. The vascular-labeled Tg(*kdrl*:mCherry-*ras*)^{s896} zebrafish line was used to visualize blood vessels[13]. Intracardiac injection with 10-kDa or 2,000-kDa Alexa Fluor 488–conjugated dextran at 3 d.p.f. was followed by live imaging. As expected, 2,000-kDa fluorescently labeled dextran was confined within the blood vessels of control-injected embryos (**Fig. 3d**, **Supplementary Fig. 10** and **Supplementary Videos 1–4**). In contrast, dextran extravasated extensively from vessels, as evidenced by fluorescence within the brain parenchyma, in *mfsd2aa*-morphant brains (36/83 embryos tested) (**Fig. 3d**, **Supplementary Fig. 10** and **Supplementary Videos 5–8**). Finally, coinjection with either zebrafish or human wild-type mRNA largely rescued dextran extravasation, whereas coinjection with human *MFSD2A* mRNA encoding the Thr159Met or Ser166Leu mutant failed to reverse extravasation (**Fig. 3d**, **Supplementary Fig. 10** and **Supplementary Videos 9–24**). Similar results were obtained with 10-kDa Alexa Fluor 488–conjugated dextran (**Supplementary Fig. 11** and **Supplementary Videos 25–36**). Moreover, 10% of brains morphant for *mfsd2aa* but not *mfsd2ab* exhibited internal hemorrhage (**Supplementary Fig. 12**), consistent with breakdown of the BBB. The similar dextran extravasation phenotypes in mice and zebrafish suggest conserved function in mediating BBB integrity, and, although we did not observe evidence of blood-derived products in T2-weighted magnetic resonance imaging (MRI) (**Supplementary Fig. 13**), the hydrocephalus may have its root in defective BBB function.

LPCs are synthesized by the liver and circulate via albumin at levels equivalent to unesterified fatty acids in plasma, and they serve as the chemical carrier for DHA uptake via MFSD2A. The specific roles for LPCs in brain growth remain only partially characterized, but their abundance in blood and efficient conversion to PC in cellular membranes suggest that they have a key role in cellular homeostasis and growth, likely involving functions in neural progenitor proliferation and neurite outgrowth[14,15]. Brain tissue from *MFSD2A*-mutated patients was not available for our studies, precluding quantification of brain DHA concentrations. Because *Mfsd2a*-knockout mice exhibit reduced transport of plasma LPCs into the brain[3], we hypothesized that plasma LPC uptake by MFSD2A at the BBB affects plasma LPC levels and that loss of MFSD2A transporter function should result in increased plasma LPC levels, which could serve as a surrogate marker for defective LPC transport. We thus quantified plasma LPC levels in *Mfsd2a*-knockout mice, which we found to be increased by 40% in comparison to controls ($P = 0.0094$; **Fig. 4a**). We found increased plasma LPC levels for the major LPC species in *Mfsd2a*-knockout mice in comparison to controls (**Fig. 4b**). Consistent with increased plasma steady-state LPC levels in *Mfsd2a*-knockout mice and with the finding that brain uptake of LPCs in *Mfsd2a*-knockout mice is reduced by 85–90%, depending on the LPC species[3], tracer studies of intravenously injected LPC-[^{14}C]oleate showed increased levels of plasma LPC-[^{14}C]oleate in *Mfsd2a*-knockout mice in comparison to controls at 2 h after injection (**Fig. 4c**). Given these results, we tested whether *MFSD2A*-mutated patients also have increased plasma levels of LPCs relative to their heterozygous parents and healthy age-matched controls. Lipidomic analysis indicated that total plasma LPC levels were increased in the probands relative to their heterozygous parents and controls (**Fig. 4d**). Similar to the findings in *Mfsd2a*-knockout mice, the levels of the common plasma LPC species containing 16:0, 18:0, 18:1 and 18:2 fatty acids were increased in the sera from *MFSD2A*-mutated patients, consistent with a defect in LPC uptake at the BBB (**Fig. 4e**). In summary, lipid analysis identified elevated serum LPC levels, likely resulting from failed cellular uptake due to lack of MFSD2A activity. Because MFSD2A can transport both DHA and other long-chain fatty acids linked to LPC[3], it remains unknown the degree to which defects in the transport of specific LPCs contribute to the disease phenotype in humans.

It has been reported that *Mfsd2a*-knockout mice have a leaky BBB resulting from increased transcytosis of pinocytotic vesicles on the luminal side of the BBB endothelium[5]. It is questionable whether leaky BBB due to transcytosis is causative in defective brain growth. Indeed, mouse models of pericyte deficiency due to mutations in *Pdgfb* have a leaky BBB resulting from markedly increased transcytosis[16–18]. However, these pericyte-deficient models do not have microcephaly. In addition, MFSD2A levels were reported to be reduced by ~40% in brain capillaries in a pericyte-deficient model, as determined by immunofluorescence microscopy, which was suggested to be a cause for the leaky BBB in pericyte deficiency[5]. However, MFSD2A levels are reduced by ~50% in *Mfsd2a*-heterozygous mice, without these mice exhibiting microcephaly[5,7]. Taken together, these findings suggest that disruption of the BBB through increased transcytosis is unlikely to cause microcephaly in *Mfsd2a*-knockout mice. Nevertheless, the leaky BBB in *Mfsd2a*-knockout mice could be a result of defective transport of LPCs into the BBB endothelium and raises the possibility that LPCs have a role in membrane integrity and function at the BBB. It will be interesting to determine whether human subjects with *MFSD2A* mutations display telltale evidence of BBB breakdown, such as small

petechial microlesions[19], but brain samples were not available from the deceased patients. Our study establishes a mechanistic association between LPC transport by MFSD2A and human brain growth and function.

METHODS

Methods and any associated references are available in the online version of the paper.

Accession codes. The exome sequencing data from individuals in this study have been deposited to the database of Genotypes and Phenotypes (dbGaP) under accession phs000288.v1.p1.

Note: Any Supplementary Information and Source Data files are available in the online version of the paper.

ACKNOWLEDGMENTS

This work was supported by grants from the US National Institutes of Health, including P01HD070494 (to J.G.G. and N.C.C.), R01NS048453 (to J.G.G.), K99NS089943 (to A.G.-G.), and U54HG003067 to the Broad Institute and U54HG006504 to the Yale Center for Mendelian Disorders (M.G.), grant CBRG/069/2014 from the Singapore Ministry of Health's National Medical Research Council (to D.L.S.), Singapore National Research Foundation Competitive Research Program grant 2007-04 (to M.R.W.) and the National University of Singapore's Life Sciences Institute (to M.R.W.). Sequencing was provided in part by a gift from BGI to Rady Children's Hospital, San Diego for undiagnosed patients. Human brain samples were provided by S. Roy (University of California, San Diego).

AUTHOR CONTRIBUTIONS

M.S.Z., M.K., T.B.-O., K.K.V. and R.O.R. recruited subjects and analyzed the clinical data. E.S., J.S. and B.C. interpreted exome results. J.G.G. and D.L.S. conceived and designed the project. N.A. prepared human brain samples. M.G. and S.G. provided sequencing. A.G.-G. performed genetic analysis to identify *MFSD2A* mutations. L.N.N. performed lipid transport studies, lipidomics, thin-layer chromatography (TLC) and confocal microscopy. H.Y. and N.C.C. performed zebrafish morpholino studies, and A.G.-G. analyzed and interpreted the data. B.R., D.Q.Y.Q., B.H.W. and B.C.T. assisted with cloning, immunoblots and imaging. A.C.-G. and M.R.W. provided expertise in mass spectrometry. D.L.S., L.N.N., A.G.-G. and J.G.G. wrote the manuscript.

COMPETING FINANCIAL INTERESTS

The authors declare no competing financial interests.

1. Svennerholm, L. Distribution and fatty acid composition of phosphoglycerides in normal human brain. *J. Lipid Res.* **9**, 570–579 (1968).
2. Söderberg, M., Edlund, C., Kristensson, K. & Dallner, G. Fatty acid composition of brain phospholipids in aging and in Alzheimer's disease. *Lipids* **26**, 421–425 (1991).
3. Nguyen, L.N. *et al.* Mfsd2a is a transporter for the essential omega-3 fatty acid docosahexaenoic acid. *Nature* **509**, 503–506 (2014).
4. Engle, P.L. *et al.* Strategies to avoid the loss of developmental potential in more than 200 million children in the developing world. *Lancet* **369**, 229–242 (2007).
5. Ben-Zvi, A. *et al.* Mfsd2a is critical for the formation and function of the blood-brain barrier. *Nature* **509**, 507–511 (2014).
6. Daneman, R. *et al.* The mouse blood-brain barrier transcriptome: a new resource for understanding the development and function of brain endothelial cells. *PLoS ONE* **5**, e13741 (2010).
7. Berger, J.H., Charron, M.J. & Silver, D.L. Major facilitator superfamily domain–containing protein 2a (MFSD2A) has roles in body growth, motor function, and lipid metabolism. *PLoS ONE* **7**, e50629 (2012).
8. Nakanishi, H. *et al.* Cloning and characterization of mouse lung-type acyl-CoA: lysophosphatidylcholine acyltransferase 1 (LPCAT1). Expression in alveolar type II cells and possible involvement in surfactant production. *J. Biol. Chem.* **281**, 20140–20147 (2006).
9. Ethayathulla, A.S. *et al.* Structure-based mechanism for Na^+/melibiose symport by MelB. *Nat. Commun.* **5**, 3009 (2014).
10. Cordat, E., Leblanc, G. & Mus-Veteau, I. Evidence for a role of helix IV in connecting cation- and sugar-binding sites of *Escherichia coli* melibiose permease. *Biochemistry* **39**, 4493–4499 (2000).
11. Fleming, A., Diekmann, H. & Goldsmith, P. Functional characterization of the maturation of the blood-brain barrier in larval zebrafish. *PLoS ONE* **8**, e77548 (2013).
12. Kok, F.O. *et al.* Reverse genetic screening reveals poor correlation between morpholino-induced and mutant phenotypes in zebrafish. *Dev. Cell* **32**, 97–108 (2015).
13. Chi, N.C. *et al.* Foxn4 directly regulates *tbx2b* expression and atrioventricular canal formation. *Genes Dev.* **22**, 734–739 (2008).
14. He, C., Qu, X., Cui, L., Wang, J. & Kang, J.X. Improved spatial learning performance of fat-1 mice is associated with enhanced neurogenesis and neuritogenesis by docosahexaenoic acid. *Proc. Natl. Acad. Sci. USA* **106**, 11370–11375 (2009).
15. Kawakita, E., Hashimoto, M. & Shido, O. Docosahexaenoic acid promotes neurogenesis *in vitro* and *in vivo*. *Neuroscience* **139**, 991–997 (2006).
16. Daneman, R., Zhou, L., Kebede, A.A. & Barres, B.A. Pericytes are required for blood-brain barrier integrity during embryogenesis. *Nature* **468**, 562–566 (2010).
17. Bell, R.D. *et al.* Pericytes control key neurovascular functions and neuronal phenotype in the adult brain and during brain aging. *Neuron* **68**, 409–427 (2010).
18. Armulik, A. *et al.* Pericytes regulate the blood-brain barrier. *Nature* **468**, 557–561 (2010).
19. Harata, N. & Iwasaki, Y. The blood-brain barrier and selective vulnerability in experimental thiamine-deficiency encephalopathy in the mouse. *Metab. Brain Dis.* **11**, 55–69 (1996).

ONLINE METHODS

Patient ascertainment. Patients were enrolled and sampled according to standard practice in approved human subject protocols at the University of California. Patients were recruited from developmental child neurology clinics throughout the Middle East, North Africa and Central Asia presenting with features of neurodevelopmental delay or regression, intellectual disability, autism, epilepsy or structural brain malformations between 2004 and 2012. Clinical records, radiographs and past history were reviewed, and patients were examined by one or more of the authors. Blood and/or saliva were collected on all potentially informative family members, upon informed consent approval and consistent with institutional review board (IRB) guidelines. DNA was extracted and subjected to quality control measures and subsequent genetic investigation.

Animals. *Mfsd2a*-knockout mice were generated as described previously[7]. Experimental protocols were approved by the SingHealth Institutional Animal Care and Use Committee. Zebrafish experiments were performed in compliance with the Institutional Animal Care and Use Committee at the University of California, San Diego.

Exome sequencing. Exome sequencing was performed on both the parents and affected member from each family. Genomic DNA was subjected to library preparation with the Agilent Human All Exon 50 Mb kit and then underwent paired-end sequencing (2 × 150 bp) on the Illumina HiSeq 2000 instrument. For each patient sample, >90% of the exome was covered at >30×. The Genome Analysis Toolkit (GATK)[20] was used for variant identification. We tested for segregating rare structural variants using XHMM[21]. We then filtered for homozygous variants using custom Python scripts (available upon request), to remove alleles with frequency >0.1% in the population[22], not occurring in homozygous intervals or without high scores for likely damage to protein function. New mutations were identified in the *MFSD2A* gene in families 1422 and 1825, where no other members of the cohort displayed putative deleterious variants.

Sanger sequencing. Primers were designed using the Primer3 program and tested for specificity using BLAST software. PCR products were treated with exonuclease I (Fermentas) and shrimp alkaline phosphatase (USB) and sequenced using BigDye Terminator Cycle Sequencing Kit v.3.1 on an ABI 3100 Genetic Analyzer (Applied Biosystems). Sequence data were analyzed with Sequencher 4.9 (Gene Codes).

Mutagenesis of *MFSD2A*. Human *MFSD2A* in pCMV-SPORT6 (Open Biosystems) was amplified using primers hMfsd2aBamHI and hMfsd2aXbaI (**Supplementary Table 6**) and cloned into pcDNA3.1 in the BamHI and XbaI sites. To generate the *MFSD2A* mutations correspond to p.Thr159Met and p.Ser166Leu by PCR, specific primers were used (**Supplementary Table 6**). The mutated PCR products encoding p.Thr159Met and p.Ser166Leu were subsequently cloned into pcDNA3.1 and sequence verified.

PNGase F treatment. Expression of wild-type MFSD2A and Thr159Met and Ser166Leu mutant MFSD2A in HEK293 cells was achieved as previously described[2] with the exception that the incubation time was 3 h. Immunoblotting was performed with previously described antibody to MFSD2A[3,7]. HEK293 cells were obtained from the American Type Culture Collection and are mycoplasma free.

Modeling of MFSD2A. The three-dimensional structure of MFSD2A was modeled using the i-Tasser program. The best-fit model for human MFSD2A was the bacterial melibiose permease MelB, for which an atomic-resolution structure was recently solved[4]. The transmembrane domains and residues of modeled MFSD2A were subsequently viewed using PyMoL.

Transport assays. Transport assays using HEK293 cells were performed as previously described[4]. Briefly, plasmids encoding wild-type, Thr159Met or Ser166Leu human MFSD2A or zebrafish Mfsd2aa or Mfsd2ab were transfected into HEK293 cells. Uptake assays were performed after 24 h of transfection with a range of concentrations for LPC-[^{14}C]DHA, LPC-[^{14}C]oleate and LPC-[^{3}H]palmitate. Experiments were repeated twice in triplicate in 12-well plates. Uptake activity was expressed as dpm/well. Radiolabeled LPC-[^{14}C]DHA, LPC-[^{14}C]oleate and LPC-[^{3}H]palmitate were purchased from ARC. Non-radiolabeled LPC-DHA was synthesized as described previously[3]. LPC-oleate and LPC-palmitate were obtained from Avanti Polar Lipids.

Thin-layer chromatography analysis of phospholipids. HEK293 cells overexpressing pcDNA3.1hMfsd2a (wild-type human MFSD2A), pcDNA3.1Mfsd2aT159M (Thr159Met MFSD2A), pcDNA3.1Mfsd2aS166L (Ser166Leu MFSD2A), zebrafish mfsd2aa or mfsd2ab, or pcDNA3.1 (mock) plasmid were washed once with serum-free DMEM before incubation with 100 µM radiolabeled LPC-[^{14}C]oleate for 30 min. Wells were washed three times with DMEM containing 0.5% BSA. Lipids were extracted twice with HIP buffer (hexanes:isopropanol; 3:2 ratio) for 30 min, dried with nitrogen stream, reconstituted in chloroform and spotted on TLC plates (Millipore). The solvent for phospholipid separation was chloroform:methanol:ammonia solution (25%; 50:25:6, per volume). TLC plates for radiolabeled phospholipids were dried for 30 min and exposed overnight to Phosphor screens, which were scanned with a Typhoon FLA 9000 scanner (Agilent Technologies). Phospholipid bands were quantified using ImageQuant software, and amounts were expressed as fold change relative to the amount in the mock-transfected control.

Lipidomic analysis of plasma samples. For human plasma samples, a single plasma sample each for the father, mother and affected individual (1.5 years old) from family 1825 and duplicate samples for the father, mother and affected individual (4.5 years old) from family 1422 were used for LPC analysis. Age-matched human plasma samples from 15 healthy children (male and female) between 0.1 and 18 years old (mean = 4.3 years; s.d. = ±4.4 years) were used as controls. Lysophospholipids were extracted using a methanol-based protocol described previously[5,23]. Briefly, plasma samples (2 µl) were resuspended in 200 µl of methanol containing 100 pmol/ml LPC 20:0 as an internal standard (Avanti Polar Lipids), and samples were vortexed for 30 s and sonicated for 30 min on ice. Samples were centrifuged at 20,000*g* for 10 min at 4 °C to remove debris. The supernatants were diluted 5× with methanol (total volume of 25 µl) before injection into a liquid chromatography–tandem mass spectrometry (LC-MS/MS) instrument. For mouse plasma samples, lysophospholipids were extracted using activated charcoal. Briefly, plasma (150 µl) from five wild-type and five *Mfsd2a*-knockout littermates aged 3.5 months, both male and female, was first diluted with 650 µl of PBS and then with 800 µl of activated charcoal solution (1 g/50 ml PBS). No randomization was performed. Samples were rotated for 1 h at 25 °C and then centrifuged for 5 min at 14,000*g* to collect the charcoal pellets. The pellets were washed three times with PBS and resuspended in 500 µl of PBS. An equal amount of chloroform:methanol (2:1) was added, and samples were rigorously vortexed for 30 min at 25 °C. The organic phase was separated by centrifugation, and lipids were extracted twice with chloroform:methanol (2:1) and dried with nitrogen gas. Before lipidomic analysis, dried lipid extracts were resuspended in 150 µl of chloroform:methanol (1:1) and further diluted with 200 µl of methanol containing 0.91 nmol/ml LPC 20:0 as an internal standard. These solutions were used for injection into the LC-MS/MS instrument.

Mass spectrometry analysis. Samples were randomized for injection into the LC-MS/MS instrument. Each sample was analyzed in technical triplicates. Analysis for each sample was followed by injection with a blank to avoid carryover. The stability of the signal throughout the analysis was monitored by regular injection of a quality control sample. Chromatographic analysis was undertaken on a 1290 Liquid Chromatography System (Agilent Technologies) using a Kinetex HILIC stationary-phase column (Phenomenex) with the following dimensions: column length, 150 mm; column internal diameter, 2.1 mm; particle size, 2.6 µm; pore size, 100 Å. Gradient elutions were performed with solvents A (95% acetonitrile/5% 10 mM ammonium formate/0.1% formic acid) and B (50% acetonitrile/50% 10 mM ammonium formate/0.1% formic acid), with a gradient range from 0.1 to 75% solvent B in 6 min, 75 to 90% solvent B in 1 min, and 90 to 0.1% solvent B in 0.1 min, followed by 0.1% solvent B for 3 min (total run time of 10.1 min). Under these conditions, LPC species eluted in ~4.9 min with a flow rate of 0.5 ml/min. LPC species were quantified using Multiple-Reaction Monitoring (MRM) on a 6460 triple-quadruple mass

doi:10.1038/ng.3311

spectrometer (Agilent Technologies) with gas temperature of 300 °C, gas flow of 5 l/min, sheath gas flow of 11 l/min and capillary voltage of 3,500 V. MRM transitions were from precursor ions to the choline head fragment (*m*/*z* (mass/charge) ratio =184) with a collision energy of 29 V. We monitored 36 transitions simultaneously with a dwell time of 20 ms. Quantification data were extracted using MassHunter Quantitative Analysis (QQQ) software, and data were manually curated to ensure correct peak integration. Areas under the curve (AUCs) for the extracted ion chromatogram peaks for each MRM transition and lipid species were normalized to the internal standard. Concentrations for total and individual LPC species from human and mouse samples were expressed in mM.

Blood LPC-[^{14}C]oleate analysis. *Mfsd2a*-knockout and wild-type mice (males; 8 weeks of age) were injected intravenously with 100 mM radioactively labeled LPC-[^{14}C]oleate. Blood samples (10 ml) were collected after 2 min (initial dose) and 2 h from the tail vein, and radioactivity was quantified by scintillation counting. The amount of plasma LPC-[^{14}C]oleate in the knockout mice was expressed as the ratio relative to wild-type samples at each time point.

***In situ* hybridization.** Whole-mount *in situ* hybridization was performed on zebrafish embryos at 1, 2 and 4 d.p.f. as described previously[6], using *mfsd2aa*, *mfsd2ab* and *elavl3* (neuronal marker) antisense RNA probes as well as *mfsd2aa* sense (negative control) RNA probe. The RNA probes were generated by PCR, using specific primers (**Supplementary Table 6**).

Morpholino-mediated knockdown and *mfsd2aa* and *MFSD2A* rescue studies. Adult male and female zebrafish (<18 months old) from wild-type (AB Tübingen) and transgenic strains were maintained under standard laboratory conditions. At least three adult pairs were used to generate embryos at 0–4 d.p.f. for each experiment. No randomization was performed. Translation-blocking antisense morpholino oligonucleotides for *mfsd2aa* and *mfsd2ab* and control (scrambled) morpholino oligonucleotide were injected into embryos at the one-cell stage. Lethality (count of immobile embryos) and microcephaly (head size measured as the distance between the eyes) phenotypes were assessed. For mRNA rescue experiments, full-length zebrafish wild-type *mfsd2aa* mRNA (50 ng; $n = 118$) and human wild-type *MFSD2A* mRNA (50 ng; $n = 135$), as well as human *MFSD2A* mRNA encoding the Thr159Met and Ser166Leu mutants (50 ng; $n = 120$ and 107, respectively), were coinjected with the morpholino ($n = 592$), as described previously[6]. Treated embryos that survived were counted and scored as rescued. The location of the morpholino binding site in human and zebrafish mRNA is shown in **Supplementary Figure 14**.

Blood-brain barrier integrity assays. For zebrafish vascular phenotypes, Tg(*kdrl*:mCherry-*ras*)^{s896} embryos were used to visualize cranial vessels[7]. Embryos at the one-cell stage were injected with 1 ng of *mfsd2aa* morpholino ($n = 467$) as described[6]. At 3 d.p.f., 10-kDa and 2,000-kDa Alexa Fluor 488–labeled dextran was injected into the heart, and fluorescence was visualized 10 min and 40 min after injection. Bright-field and confocal fluorescence microscopy were used to determine whether the experimental embryos exhibited vascular dextran extravasation.

Statistical analysis. All *in vitro* experiments were performed in quadruplicate. Data are expressed as means with standard errors. We used Student's *t* test to perform between-group comparisons (two-tailed) and Tukey's test in conjunction with analysis of variance for multiple comparisons. Kaplan-Meier curves were generated for survival, and survival curves were compared using log-rank (Mantel-Cox) tests. All *P* values were tested as two-sided, and $P < 0.05$ was considered to be indicative of statistical significance after appropriate correction for multiple comparisons. No statistical methods were used to predetermine sample sizes. Experimental sample size was determined empirically from previous experimental experience with similar assays and/or from sizes generally employed in the field. Observers were not blinded to conditions.

20. DePristo, M.A. *et al.* A framework for variation discovery and genotyping using next-generation DNA sequencing data. *Nat. Genet.* **43**, 491–498 (2011).
21. Fromer, M. *et al.* Discovery and statistical genotyping of copy-number variation from whole-exome sequencing depth. *Am. J. Hum. Genet.* **91**, 597–607 (2012).
22. Tennessen, J.A. *et al.* Evolution and functional impact of rare coding variation from deep sequencing of human exomes. *Science* **337**, 64–69 (2012).
23. Shui, G. *et al.* Comparative plasma lipidome between human and cynomolgus monkey: are plasma polar lipids good biomarkers for diabetic monkeys? *PLoS ONE* **6**, e19731 (2011).